








Cite this: *Nanoscale*, 2018, **10**, 18315

Improved performance of CsPbBr₃ perovskite light-emitting devices by both boundary and interface defects passivation†

Li Song,^{a,b} Xiaoyang Guo,  *^a Yongsheng Hu,  ^a Ying Lv,  ^a Jie Lin,  ^a Yi Fan,^a Nan Zhang^a and Xingyuan Liu  *^a

Significantly enhanced luminance and current efficiency for inorganic light-emitting devices have been obtained by tetrabutylammonium bromide (TBAB) additive into perovskite precursors. Reduced non-radiative defects primarily passivated by TBAB and increased exciton binding energy are responsible for improvement of PeLED performance. By employing a TBAB-treated interfacial layer, interface defects are reduced and it results in further promotion of electroluminescence performance of PeLED, including turn-on voltage of 2.6 V, brightness as high as 67 300 cd m⁻², current efficiency of 22.5 cd A⁻¹ and external quantum efficiency of 6.28%. Our results shed light on optimization of inorganic PeLEDs by focusing on the removal of defects both at the grain boundaries and the interfaces between carrier transport layers and perovskite emitting layers.

Received 6th August 2018,
Accepted 10th September 2018

DOI: 10.1039/c8nr06311g

rsc.li/nanoscale

Introduction

Recently, metal halide perovskites have stimulated scientific interest in the field of optoelectronics, such as in photovoltaic solar cells,¹ detectors,² field effect transistors³ and light-emitting diodes,^{4,5} due to their superior optical and electrical characteristics including high absorption coefficients, high photoluminescence (PL) quantum efficiency, long diffusion length and high mobility.^{6,7} Their facile solution processability, abundant colors covering visible and infrared spectrum regions, and high color purity render them potentially applicable in displays and communications.^{8–10}

In the past few years, organic–inorganic lead halide (MAPbX₃ with X = I, Br, Cl; MA = CH₃NH₂) based perovskite light-emitting diodes (PeLEDs) have been widely studied and significant advances have been made with state-of-art performance, reaching high current efficiency (CE) of 42.9 cd A⁻¹ and high external quantum efficiency (EQE) of 8.53% for visible PeLEDs and 11.7% for infrared PeLEDs.^{11,12} However, poor

environmental stability of organic–inorganic hybrid PeLEDs still remains an obstacle for long term applications.^{13,14} Recently, all-inorganic perovskite CsPbX₃ (X = Cl, Br, I) as an indispensable supplementary component has shown better thermal and chemical stability.^{15–17} Therefore, PeLEDs based on all-inorganic halide perovskites are promising candidates to realize high performance and stability.

Since the first reported inorganic PeLED, efforts have mainly focused on two forms, synthesized nanocrystals and regulated bulk films, to improve performance of PeLEDs. The former usually have advantages in high photoluminescence quantum yield (PLQY) and color tunability *via* controlling the size of nanocrystals and mixing different halide compounds with varied stoichiometric ratios.^{9,18–21} However, the complicated synthesis process (often containing several cycles of centrifugation) requiring long insulating ligands (hindering charge injection to the nanocrystals) are drawbacks to achieving efficient PeLEDs. In contrast, the facile one step solution process method for perovskite film growth can circumvent these problems and has potential to realize efficient PeLEDs. Tiny crystal grains are considered to be necessary to reduce exciton diffusion and inhibit exciton dissociation into free carriers, which will improve luminescent properties. Concomitant with reduced crystal grains, more surface trap states among grain interfaces (metallic Pb atoms or halogen vacancies) will appear due to high densities of grain boundaries, which may trap charges and result in nonradiative recombination. Both reduced nanocrystal defects and surface defects at grain boundaries would compete with each other to

^aState Key Laboratory of Luminescence and Applications, Changchun Institute of Optics, Fine Mechanics and Physics, Chinese Academy of Sciences, Changchun 130033, China. E-mail: guoxy@ciomp.ac.cn, liuxy@ciomp.ac.cn

^bUniversity of Chinese Academy of Sciences, Beijing 100049, China

†Electronic supplementary information (ESI) available: XPS, PL spectra, ATR-FTIR spectra, XRD patterns, capacity density, SEM images, and work function for PEDOT:PSS films; optical and electrical performances for PeLED with CB:DMSO treated PEDOT:PSS, device stability, additional tables. See DOI: 10.1039/c8nr06311g

realize optimal device performance. To minimize defect state densities, one strategy is to blend perovskite precursors with additives. Polymer dielectrics are traditional additives, such as poly(ethylene oxide),^{16,22} poly(2-ethyl-2-oxazoline),²³ and polyethylene glycol,²⁴ which have been broadly used in both MAPbX₃ and CsPbX₃ systems. Another type of additive is amine-based passivating materials,²⁵ which have recently been investigated in MAPbX₃ and have been seldom adopted in CsPbX₃ PeLEDs.

Besides structural defects of the perovskite film itself, properties of the adjacent charge transport layer, especially the underlayer on which perovskite is deposited, play a crucial role in device performance. There often exists a charge injection barrier between the charge transport layer and perovskite emissive layer, together with exciton quenching centers at the interface, which restrict electroluminescence (EL) performance.^{26–28} A prevalent approach to address this issue is to introduce interfacial layers. Moreover, modification by interfacial layer can significantly influence growth of perovskite layers due to change in surface energy and passivation of luminescent quenching centers.^{4,27} Consequently, EL performance can be drastically improved. Essentially, reducing defects both in the perovskite film and at the interface is crucial to improving EL performance of PeLEDs.

Herein, we introduce an easily accessible Lewis base amine-based passivating material tetrabutylammonium bromide (TBAB) in the preparation of inorganic CsPbBr₃ light-emitting diodes for the purpose of passivating defects originating from Pb atoms. TBAB impedes growth of CsPbBr₃ crystals and acts as an adhesive to conglutinate the small grains. Enhanced light-emitting intensity as well as prolonged exciton decay lifetime demonstrate the drastically decreased nonradiative

defects. Temperature-dependent PL intensity measurement shows that exciton binding energy is also increased in TBAB:CsPbBr₃ film. Treatment of poly(ethylenedioxythiophene):poly(styrenesulfonate) (PEDOT:PSS) by TBAB further reduces interfacial defects between PEDOT:PSS and perovskite emission layer. These merits substantially improve device performance, resulting in an optimal PeLED with turn-on voltage (V_{on}) of 2.6 V, brightness as high as 67 300 cd m⁻² and CE of 22.5 cd A⁻¹. Our results provide a positive approach to optimization of inorganic PeLEDs by amine-based passivating additive.

Fig. 1a displays the multilayer device structure of the PeLED, including PEDOT:PSS (40 nm) as hole transport layer, CsPbBr₃ or TBAB:CsPbBr₃ as emission layer, 1,3,5-tris(*N*-phenyl-benzimidazol-2-yl) benzene (TPBi, 30 nm) as electron transport and hole blocking layer, and LiF/Al as top cathode. To gain optimal optoelectronic performance, different amounts of TBAB were incorporated into CsPbBr₃ to fabricate PeLEDs with TBAB weight ratios of 0%, 2.3%, 3.4%, 4.6% and 5.2%. As shown in Fig. 1b–d, the control device without TBAB doping in the CsPbBr₃ emission layer shows a V_{on} of 3.1 V, maximum luminance of 1450 cd m⁻² at 7.8 V, maximum CE of 1.33 cd A⁻¹ and maximum EQE of 0.37%. As increasing amounts of TBAB were added to the CsPbBr₃ precursor solution, the brightness, CE and EQE values gradually improved, and achieved optimized device performance at TBAB weight ratio of 4.6%, which shows a V_{on} of 2.8 V, maximum luminance of 28 100 cd m⁻² at 6.3 V, maximum CE of 15.4 cd A⁻¹ and maximum EQE of 4.3%. Decreased device performance was observed with further increased TBAB ratio of 5.2%. EL spectra (Fig. 1f) of the device exhibit a sharp emission peak centered around 520 nm with a full width at half-maximum (FWHM) of 18 nm and represents no peak drift as voltage

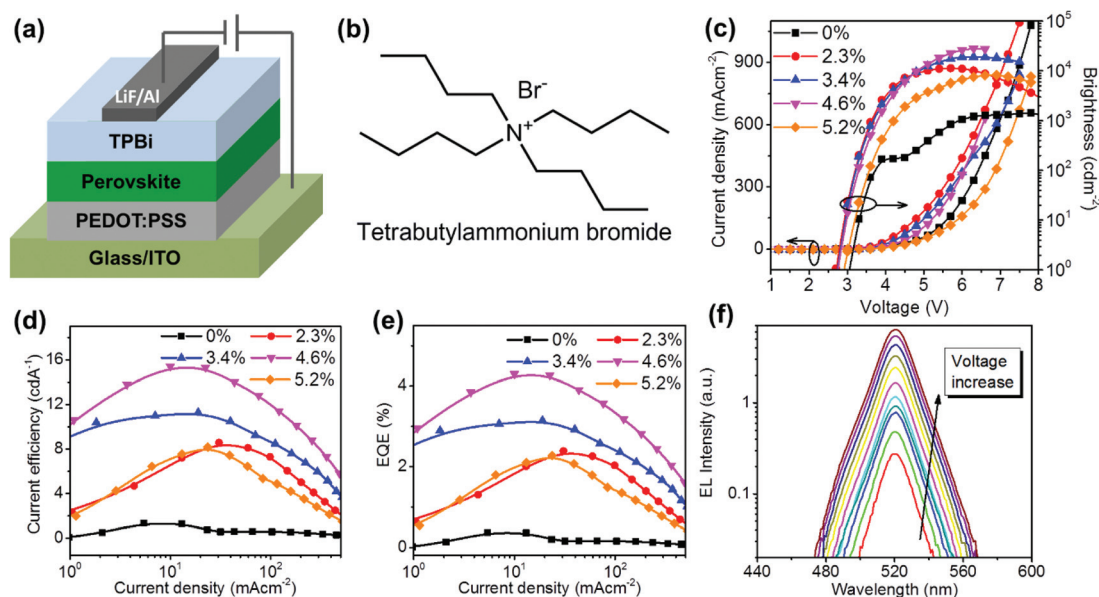


Fig. 1 (a) Schematic of multilayer PeLED. (b) Molecular structure of TBAB. (c) J - V and L - V , (d) CE- J , and (e) EQE- J curves for PeLEDs with different TBAB-doping weight ratios. (f) EL spectra of PeLED with TBAB-doping weight ratio of 4.6% under voltages from 3 V to 6 V with step of 0.3 V.

varies from 3 V to 6 V, ensuring pure color rendering ability, which is conducive to flat panel display technologies.

Surface binding states of the perovskite films were investigated by X-ray photoelectron spectroscopy (XPS). XPS survey spectra (Fig. S1a†) exhibit strong Br (*ca.* 68 eV), Pb (*ca.* 138 and 143 eV) and Cs (*ca.* 724 eV and 738 eV) peaks, indicating a well-fabricated CsPbBr₃ layer. High-resolution XPS spectrum of TBAB:CsPbBr₃ composite film (Fig. S1b†) presents a signal of N 1s at ~402 eV, which verified the existence of TBAB in the TBAB:CsPbBr₃ composite film, compared with no observed N 1s in pure CsPbBr₃ film. Furthermore, identical oxidation Pb 4f and Br 3d spectra for samples both with and without TBAB additive (Fig. S1c–e†) demonstrate that TBAB did not incorporate into the CsPbBr₃ lattice, which was also verified by the observed X-ray diffraction (XRD) patterns and PL spectra (Fig. S2†). Other than the two main peaks in the Pb 4f spectra at 142.7 eV (4f 5/2) and 137.9 eV (4f 7/2) as reported in other researches, the lower binding energy usually assigned to metallic Pb signal^{11,29} is not observed in our samples, since the excessive CsBr in CsBr:PbBr₂ (molar ratio 1.86:1) precursor solutions suppressed formation of unsaturated Pb states, which would act as quenching centers and lower EL efficiency.

Scanning electron microscopy (SEM) was performed to understand the role of TBAB in improving the device performance. Fig. 2a and b display perovskite films fabricated by the one-step solution spin-coating method on ITO/PEDOT:PSS substrates. As can be seen from the SEM image in Fig. 2, grain size of perovskite after TBAB doping appears enlarged in contrast to that of pure CsPbBr₃ film. The high resolution SEM

image demonstrates that the large grains are primarily composed of smaller ones, as shown in the inset of Fig. 2b. TBAB impedes the growth of CsPbBr₃, which resembles other reported bulk alkyl ammonium salts^{30–32} and acts as an adhesive to conglomerate small grains into a big one.

Ultraviolet-visible (UV-vis) absorption and steady-state PL spectroscopy were carried out to study the effect of TBAB on optical characteristics of perovskite films. As shown in Fig. 2c, similar absorption onsets and PL spectra were observed in both CsPbBr₃ and TBAB:CsPbBr₃ films. There exists a small red shift (~3 nm) in both absorption and PL spectra of TBAB:CsPbBr₃ film. Such red-shift phenomena have been observed previously and can be attributed to composition change at grain boundaries,³³ crystallinity changes,³⁴ photon re-absorption/recycling effect,^{35,36} lattice strain,³⁷ or chemical composition variations.^{38,39} Different from other organo-ammonium halides,^{38,39} TBA⁺ has a larger ionic radius than nonvalent *n*-butylammonium cation, which often serves as the spacer in quasi-2D perovskite materials. Hence, TBA⁺ should not partially substitute Cs⁺ and subsequently form a new alloy perovskite phase. We failed to obtain the gradually red-shifted spectrum when changing TBAB weight ratios (Fig. S2a†), demonstrating that chemical composition change in the perovskite crystal is not the origin of red-shift in the PL spectrum. No observable change in XRD spectra between pure CsPbBr₃ and TBAB:CsPbBr₃ films (Fig. S2b†) also excludes composition changes in perovskite crystal. Furthermore, attenuated total reflectance infrared (ATR-FTIR) spectroscopy demonstrated that TBAB can interact with Pb atoms (Fig. S3†). Therefore, we

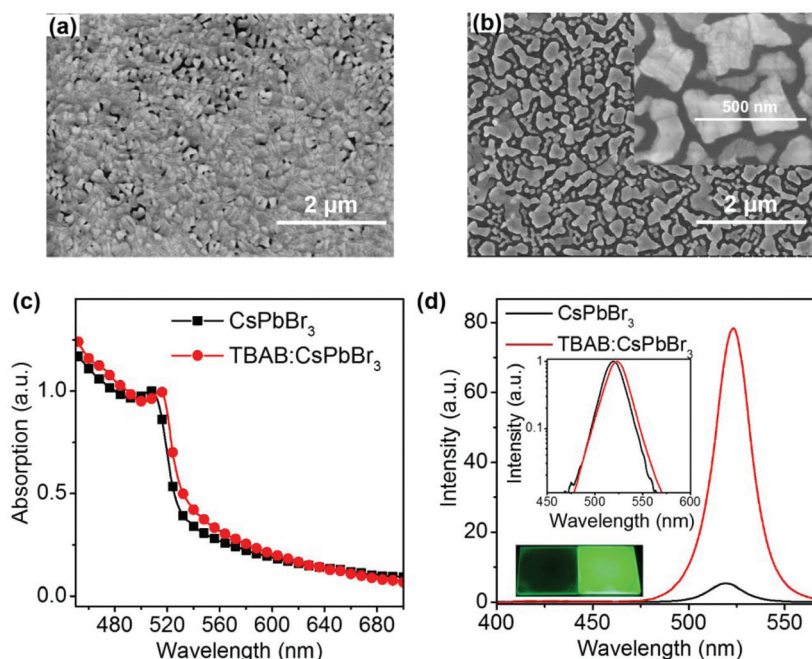


Fig. 2 SEM images for (a) pure CsPbBr₃ film and (b) TBAB:CsPbBr₃ film (weight ratio 4.6%) (inset is corresponding high resolution SEM image), (c) absorption and (d) PL spectra for pure CsPbBr₃ and TBAB:CsPbBr₃ films. Insets are normalized spectra and film photographs under UV light (left: CsPbBr₃, right: TBAB:CsPbBr₃).

deduce that TBAB mainly passivates CsPbBr₃ crystal surface at grain boundaries and this resulted in the red-shifted PL emission. Concomitant with the red-shift, significant improvement in PL (see photograph in Fig. 2d) was observed in TBAB:CsPbBr₃ film (PLQY of ~42%) in comparison to that of the pristine CsPbBr₃ film (PLQY of ~1.5%).

PL decay curves for both pure CsPbBr₃ film and TBAB-doped CsPbBr₃ film were measured to investigate defects of the films, as shown in Fig. 3a. Transient PL decay measurements reveal that TBAB:CsPbBr₃ film possesses a much longer average lifetime of ~102.0 ns in comparison to ~14.8 ns for pure CsPbBr₃ film. The drastically enhanced PL emission intensity and greatly prolonged average lifetime indicate significantly decreased nonradiative defects in TBAB:CsPbBr₃ film, which can be ascribed to efficient passivation by TBAB beneficial to EL enhancement.

Exciton binding energy (E_b) is a key physical parameter relevant to charge transfer and exciton dissociation probability in the PL process. Temperature-dependent PL intensity measurement was carried out to investigate the difference in E_b for different perovskite films. PL spectra of pure CsPbBr₃ and TBAB:CsPbBr₃ (Fig. 3b) were measured at temperatures ranging from 45 K to 265 K. Blue-shifted PL spectra and broadened linewidth were observed in both CsPbBr₃ and TBAB:CsPbBr₃ films as temperature increased (Fig. S4†), which is in conformity with previous reports.^{9,40} Decrease in PL intensity as temperature increases can be attributed to enhanced thermal dissociation of excitons. E_b values can be extracted with a fit using the following equation:

$$I(T) = I_0 / (1 + A \exp(-E_b/k_B T)) \quad (1)$$

where I_0 and k_B represent the initial PL intensity and Boltzmann's constant, respectively. The fitted E_b are 37 and 47 meV for pristine CsPbBr₃ and TBAB:CsPbBr₃ films, respectively. The experimental value for pristine CsPbBr₃ film is consistent with the previously reported value of bulk CsPbBr₃ (35 meV).⁴¹ A higher value than that of the thermal disturbance energy at room temperature (~26 meV) guarantees efficient exciton generation and recombination and therefore intensive light emission. In contrast to CsPbBr₃ film, higher

E_b for TBAB:CsPbBr₃ film indicates larger electron-hole wavefunction overlap leading to weaker exciton dissociation probability and stronger light emission capability, which agrees well with the enhancement in PLQY and is beneficial to realizing outstanding CsPbBr₃ PeLEDs with high efficiency. For the bulk material, E_b can be expressed by

$$E_b = \mu e^4 / (2\epsilon^2 \hbar^2) \quad (2)$$

where μ , e , ϵ and \hbar denote exciton reduced mass, elementary charge, dielectric constant and reduced Planck constant, respectively.⁴² The increase in E_b for TBAB:CsPbBr₃ may originate from variation in the dielectric constant after TBAB doping, which was verified by the capacitance measurement shown in Fig. S5.† In addition, the electronic band gap equals the sum of the optical band gap and E_b . Therefore, the red shift for both absorption and PL peaks for TBAB:CsPbBr₃ film is in line with the increased E_b , leading to narrowed optical band gap.

Further improvement of device performance was realized through PEDOT:PSS treatment with TBAB in chlorobenzene (CB) and dimethyl sulfoxide (DMSO) mixed solvent. Fig. 4 shows the EL performance of PeLEDs with TBAB-treated PEDOT:PSS interfacial layers and the corresponding device parameters are listed in Table 1. As can be seen from Fig. 4a–c and Table 1, for each amount of TBAB doping, devices with TBAB interfacial treatment show improved luminance and efficiency. The optimized device displays a maximum brightness of 67 300 cd m⁻², CE of 22.5 cd A⁻¹ and EQE of 6.28%. Reproducibility of the best performance was evaluated by 39 separate devices, as shown in the histogram (Fig. 4d). Brightness of all devices exceeds 50 000 cd m⁻². Such performances are among the best reported for inorganic PeLEDs with a thin CsPbBr₃ layer, as shown in Table S1.†

No great differences can be observed in the morphology of TBAB:CsPbBr₃ after PEDOT:PSS was treated by TBAB (Fig. S6†), indicating that enhanced EL performance does not originate from changes in perovskite morphology. The work function of PEDOT:PSS after TBAB treatment was about -5.13 eV, which is very close to that of PEDOT:PSS before TBAB treatment (-5.19 eV) (Fig. S7†) and agrees well with the reported values.^{43–46}

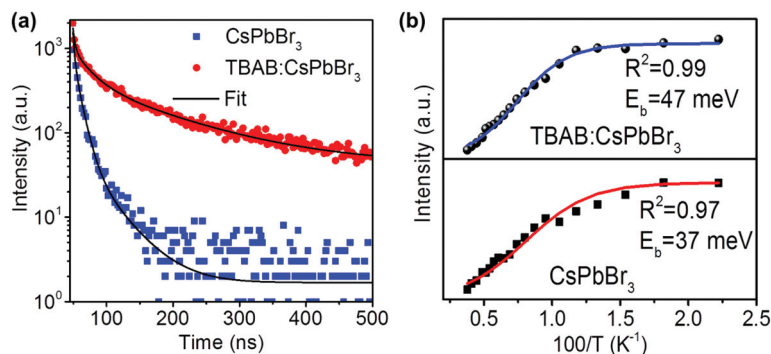


Fig. 3 (a) PL decay curves for pure CsPbBr₃ and TBAB:CsPbBr₃ films. (b) PL intensities of pristine CsPbBr₃ and TBAB:CsPbBr₃ films at temperatures ranging 45–265 K. R^2 is the coefficient of determination.

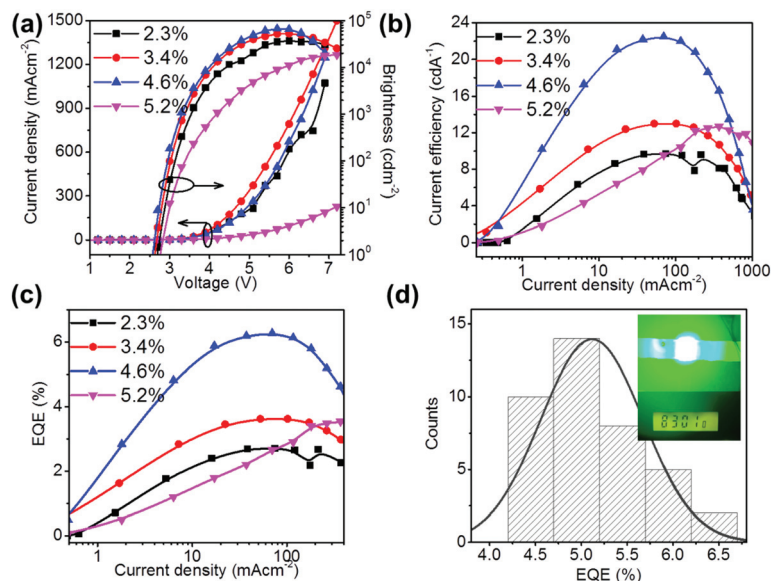


Fig. 4 (a) J - V and L - V , (b) CE - J , and (c) EQE - J curves for PeLED with different TBAB-doping ratios and TBAB treatments on PEDOT:PSS. (d) Histogram of peak EQEs measured from 39 devices. Inset is the lighted PeLED under working conditions.

Table 1 Summary of EL characteristics for PeLEDs

TBAB weight ratio	TBAB treatment	Max. luminance (cd m^{-2})	Max. CE (cd A^{-1})	Max. EQE (%)	V_{on} (V)	Voltage @ max. luminance (V)
0%	W/o	1450	1.33	0.37	3.1	7.8
2.3%	W/o	11 300	8.58	2.39	2.7	5.7
	With	37 100	9.71	2.71	2.7	6.0
3.4%	W/o	19 100	11.3	3.15	2.8	6.0
	With	52 900	13.0	3.63	2.6	6.0
4.6%	W/o	28 100	15.4	4.30	2.8	6.3
	With	67 300	22.5	6.28	2.6	5.7
5.2%	W/o	8250	8.16	2.27	2.8	6.9
	With	18 600	12.7	3.54	2.8	7.2

In addition, to test the effect of solvent treatment on PEDOT:PSS film as it would probably result in the augmentation of device performance, a control device with a PEDOT:PSS layer treated by CB:DMSO mixed solvent (10:1 v/v) was prepared, and its mediocre device performance (maximum brightness of $28\,200\text{ cd m}^{-2}$, CE of 13.4 cd A^{-1} and EQE of 3.74%) verified the positive effect of TBAB at the interface (Fig. S8†). Therefore, we infer that the main reason for further improvement in EL performance after PEDOT:PSS treatment with TBAB may come from further decrease in nonradiative defects existing at the PEDOT:PSS/perovskite interface. Transient photovoltage measurements correlated to carrier lifetime in the absorber were carried out on PeLEDs with and without PEDOT:PSS interfacial treatment to elucidate the interface, as shown in Fig. 5. It is found that the device with TBAB-treated PEDOT:PSS shows prolonged carrier lifetime of 1.48 ms (monoexponential decay fit) compared with 0.89 ms for the without TBAB treated device, indicating decreased trap state densities in TBAB-treated PeLEDs. Therefore, the PeLED with TBAB interfacial treatment exhibits superior luminance, current efficiency and decreased V_{on} .

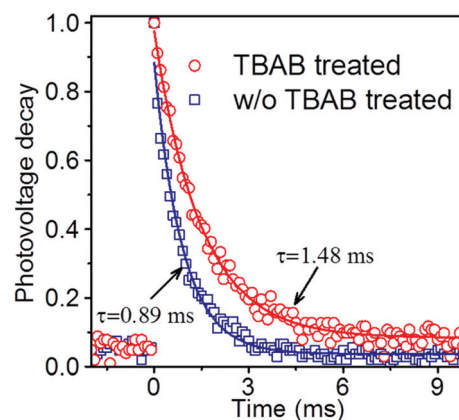


Fig. 5 Transient photovoltage decay of TBAB:CsPbBr₃ PeLEDs with and without PEDOT:PSS treatment by TBAB.

Since stability of the PeLED is related to defects existing in the interfaces and boundaries, it is expected that the PeLED with TBAB-modified CsPbBr₃ emission layer will have a longer

lifespan. We monitored decay of unencapsulated devices under ambient atmosphere (30 °C, 40% relative humidity) and constant electrical-driven conditions (Fig. S9†). Although the PeLED with pure CsPbBr₃ film shows a much shorter lifetime than in other reports,^{16,19} which might originate from exposure in air during device preparation and testing, the PeLED with TBAB-doped CsPbBr₃ film shows significantly prolonged stability under the same conditions, demonstrating the role of TBAB in passivating CsPbBr₃ film defects. Device stability was further increased after including PEDOT:PSS treated by TBAB, which is consistent with TPV results.

Although performance has been improved significantly, the imperfect and discontinuous TBAB:CsPbBr₃ film probably restricts performance to some degree. We believe EL performance would improve if a condensed TBAB:CsPbBr₃ film was formed. Efforts are still needed to ameliorate the quality of TBAB-doped perovskite film and further study the related mechanism.

In summary, luminance and CE of inorganic PeLEDs were dramatically improved by introduction of TBAB into CsPbBr₃ perovskite emission layers. The structure-directing role of TBAB conglomerates small grains into larger ones with decreased boundary nonradiative defect state density and increased exciton binding energy, which significantly enhances luminescent properties of TBAB:CsPbBr₃ composite films. By further interfacial modification of PEDOT:PSS with TBAB to remove interfacial defects, an optimized EL performance with V_{on} of 2.6 V, brightness as high as 67 300 cd m⁻², CE of 22.5 cd A⁻¹ and an EQE of 6.28% were achieved. These results highlight the importance of reducing both grain boundary defects and interfacial defects to promote EL performance of inorganic PeLEDs. This study also contributes useful suggestions to develop high performance PeLEDs with amine-based passivating materials.

Experimental methods

Materials

PbBr₂ (99.9%), CsBr (99.9%), PEDOT:PSS and TPBi were purchased from Xi'an Polymer Light Technology Corp. TBAB (99%) was purchased from Macklin. All materials were used as received without further purification.

Film fabrication and characterization

Perovskite precursor solution was prepared by blending PbBr₂ and CsBr (molar ratio 1 : 1.86) in anhydrous DMSO at a fixed concentration of 145 mg mL⁻¹. TBAB was dissolved in DMSO with the concentration of 20 mg mL⁻¹. Precursors and TBAB solutions were mixed at desired weight ratio before use. For SEM (Hitachi S-4800) characterization, perovskite films were spun on ITO/PEDOT:PSS substrates (5500 rpm, 60 s). Absorption spectra of neat perovskite and TBAB:CsPbBr₃ composite films (on quartz substrates) were performed with a Shimadzu UV-3101PC UV-vis-NIR spectrophotometer. Steady-state PL spectra were measured using Hitachi fluorescence

spectrometer F-7000. Temperature dependent PL spectra were measured with AvaSpec-ULS2048L fiber spectrometer using 340 nm laser excitation source and a liquid helium system. Transient PL decay properties and PLQY were performed by Edinburgh FLS920 spectrometer. Transient photovoltage measurement was carried out with a pulse laser (355 nm, duration of ~1 ns) and collected by Tektronix DPO5140 digital phosphor oscilloscope. ATR-FTIR spectra were obtained from EXCALIBUR spectrometer.

Device fabrication and characterization

ITO-patterned glass substrates were ultrasonically cleaned with acetone, alcohol, and deionized water sequentially and then treated with UV-ozone for 20 min. PEDOT:PSS (Clevios P AI 4083) (~40 nm) was spin-coated on the ITO and baked at 140 °C for 20 min on a hotplate under ambient air. TBAB (decomposed at ~150 °C) dissolved in chlorobenzene and DMSO (10 : 1 v/v) at 2 mg mL⁻¹ was spun on PEDOT:PSS at 5000 rpm and then annealed at 140 °C for 5 min. Then the mixed TBAB and perovskite precursor solution at the desired weight ratio was spin-coated at 5500 rpm for 60 s and annealed at 70 °C for 10 min in a N₂ filled glove box. Thickness of the perovskite layer as determined by surface profiler Ambios XP-1 is ~30 nm. Subsequently, TPBi (40 nm), LiF (1 nm) and Al (60 nm) were successively thermally evaporated at rates of 1, 0.5, and 4 Å s⁻¹, respectively. Active area of the PeLED is 0.015 cm². Brightness and current density of PeLEDs were measured using a Keithley 2400 source meter and luminance meter KONICA MINOLTA LS-110. Electroluminescence spectra were measured by AvaSpec-ULS2048L fiber spectrometer. EQE was calculated from the brightness, current and EL emission spectrum assuming Lambertian emission. Capacity density measurement was carried out on a Keithly 4200 SCS. All device measurements were carried out in air without encapsulation.

Conflicts of interest

The authors declare no competing financial interest.

Acknowledgements

This study is supported by the CAS Innovation Program, the National Natural Science Foundation of China No. 61774154, 51503196, 61704170 and 61775211, the Jilin Province Science and Technology Research Project No. 20180201029GX, 20170101039JC, 20160520176JH, and 20160520092JH, and project supported by Dawn Talent Training Program of CIOMP.

References

- 1 Y.-C. Zhao, W.-K. Zhou, X. Zhou, K.-H. Liu, D.-P. Yu and Q. Zhao, *Light: Sci. Appl.*, 2017, **6**, e16243.
- 2 L. Gu and Z. Fan, *Light: Sci. Appl.*, 2017, **6**, e17090.

- 3 T. Matsushima, S. Hwang, A. S. D. Sandanayaka, C. Qin, S. Terakawa, T. Fujihara, M. Yahiro and C. Adachi, *Adv. Mater.*, 2016, **28**, 10275–10281.
- 4 Y.-H. Kim, H. Cho and T.-W. Lee, *Proc. Natl. Acad. Sci. U. S. A.*, 2016, **113**, 11694–11702.
- 5 Q. Shan, J. Song, Y. Zou, J. Li, L. Xu, J. Xue, Y. Dong, B. Han, J. Chen and H. Zeng, *Small*, 2017, **13**, 1701770.
- 6 B. R. Sutherland and E. H. Sargent, *Nat. Photonics*, 2016, **10**, 295–302.
- 7 S. D. Stranks, G. E. Eperon, G. Grancini, C. Menelaou, M. J. P. Alcocer, T. Leijtens, L. M. Herz, A. Petrozza and H. J. Snaith, *Science*, 2013, **342**, 341–344.
- 8 F. Zhang, H. Z. Zhong, C. Chen, X. G. Wu, X. M. Hu, H. L. Huang, J. B. Han, B. S. Zou and Y. P. Dong, *ACS Nano*, 2015, **9**, 4533–4542.
- 9 X. Li, Y. Wu, S. Zhang, B. Cai, Y. Gu, J. Song and H. Zeng, *Adv. Funct. Mater.*, 2016, **26**, 2435–2445.
- 10 N. K. Kumawat, A. Dey, A. Kumar, S. P. Gopinathan, K. L. Narasimhan and D. Kabra, *ACS Appl. Mater. Interfaces*, 2015, **7**, 13119–13124.
- 11 H. Cho, S.-H. Jeong, M.-H. Park, Y.-H. Kim, C. Wolf, C.-L. Lee, J. H. Heo, A. Sadhanala, N. Myoung, S. Yoo, S. H. Im, R. H. Friend and T.-W. Lee, *Science*, 2015, **350**, 1222–1225.
- 12 N. Wang, L. Cheng, R. Ge, S. Zhang, Y. Miao, W. Zou, C. Yi, Y. Sun, Y. Cao, R. Yang, Y. Wei, Q. Guo, Y. Ke, M. Yu, Y. Jin, Y. Liu, Q. Ding, D. Di, L. Yang, G. Xing, H. Tian, C. Jin, F. Gao, R. H. Friend, J. Wang and W. Huang, *Nat. Photonics*, 2016, **10**, 699–704.
- 13 J. C. Yu, D. W. Kim, D. Bin Kim, E. D. Jung, J. H. Park, A.-Y. Lee, B. R. Lee, D. Di Nuzzo, R. H. Friend and M. H. Song, *Adv. Mater.*, 2016, **28**, 6906–6913.
- 14 O. A. Jaramillo-Quintero, R. S. Sanchez, M. Rincon and I. Mora-Sero, *J. Phys. Chem. Lett.*, 2015, **6**, 1883–1890.
- 15 Q. Shan, J. Li, J. Song, Y. Zou, L. Xu, J. Xue, Y. Dong, C. Huo, J. Chen, B. Han and H. Zeng, *J. Mater. Chem. C*, 2017, **5**, 4565–4570.
- 16 Y. Ling, Y. Tian, X. Wang, J. C. Wang, J. M. Knox, F. Perez-Orive, Y. Du, L. Tan, K. Hanson, B. Ma and H. Gao, *Adv. Mater.*, 2016, **28**, 8983–8989.
- 17 Z. Wei, A. Perumal, R. Su, S. Sushant, J. Xing, Q. Zhang, S. T. Tan, H. V. Demir and Q. Xiong, *Nanoscale*, 2016, **8**, 18021–18026.
- 18 D. Amgar, S. Aharon and L. Etgar, *Adv. Funct. Mater.*, 2016, **26**, 8576–8593.
- 19 L. Wang, N. E. Williams, E. W. Malachosky, J. P. Otto, D. Hayes, R. E. Wood, P. Guyot-Sionnest and G. S. Engel, *ACS Nano*, 2017, **11**, 2689–2696.
- 20 J. Song, J. Li, X. Li, L. Xu, Y. Dong and H. Zeng, *Adv. Mater.*, 2015, **27**, 7162–7167.
- 21 J. Li, L. Xu, T. Wang, J. Song, J. Chen, J. Xue, Y. Dong, B. Cai, Q. Shan, B. Han and H. Zeng, *Adv. Mater.*, 2017, **29**, 1603885.
- 22 J. Li, S. G. R. Bade, X. Shan and Z. Yu, *Adv. Mater.*, 2015, **27**, 5196–5202.
- 23 H. Lin, L. Zhu, H. Huang, C. J. Reckmeier, C. Liang, A. L. Rogach and W. C. H. Choy, *Nanoscale*, 2016, **8**, 19846–19852.
- 24 L. Song, X. Guo, Y. Hu, Y. Lv, J. Lin, Z. Liu, Y. Fan and X. Liu, *J. Phys. Chem. Lett.*, 2017, **8**, 4148–4154.
- 25 S. Lee, J. H. Park, B. R. Lee, E. D. Jung, J. C. Yu, D. Di Nuzzo, R. H. Friend and M. H. Song, *J. Phys. Chem. Lett.*, 2017, **8**, 1784–1792.
- 26 Y.-K. Chih, J.-C. Wang, R.-T. Yang, C.-C. Liu, Y.-C. Chang, Y.-S. Fu, W.-C. Lai, P. Chen, T.-C. Wen, Y.-C. Huang, C.-S. Tsao and T.-F. Cuo, *Adv. Mater.*, 2016, **28**, 8687–8694.
- 27 J. Wang, N. Wang, Y. Jin, J. Si, Z.-K. Tan, H. Du, L. Cheng, X. Dai, S. Bai, H. He, Z. Ye, M. L. Lai, R. H. Friend and W. Huang, *Adv. Mater.*, 2015, **27**, 2311–2316.
- 28 H. Cho, C. Wolf, J. S. Kim, H. J. Yun, J. S. Bae, H. Kim, J.-M. Heo, S. Ahn and T.-W. Lee, *Adv. Mater.*, 2017, **29**, 1700579.
- 29 X. Zhao, B. Zhang, R. Zhao, B. Yao, X. Liu, J. Liu and Z. Xie, *J. Phys. Chem. Lett.*, 2016, **7**, 4259–4266.
- 30 L. Zhao, Y.-W. Yeh, N. L. Tran, F. Wu, Z. Xiao, R. A. Kerner, Y. L. Lin, G. D. Scholes, N. Yao and B. P. Rand, *ACS Nano*, 2017, **11**, 3957–3964.
- 31 Z. Xiao, R. A. Kerner, L. Zhao, N. L. Tran, K. M. Lee, T.-W. Koh, G. D. Scholes and B. P. Rand, *Nat. Photonics*, 2017, **11**, 108–115.
- 32 M. Yuan, Q. Li Na, R. Comin, G. Walters, R. Sabatini, O. Voznyy, S. Hoogland, Y. Zhao, E. M. Beaugregard, P. Kanjanaboos, Z. Lu, D. H. Kim and E. H. Sargent, *Nat. Nanotechnol.*, 2016, **11**, 872–877.
- 33 W. Nie, H. Tsai, R. Asadpour, J.-C. Blancon, A. J. Neukirch, G. Gupta, J. J. Crochet, M. Chhowalla, S. Tretiak, M. A. Alam, H.-L. Wang and A. D. Mohite, *Science*, 2015, **347**, 522–525.
- 34 V. D'Innocenzo, A. R. S. Kandada, M. De Bastiani, M. Gandini and A. Petrozza, *J. Am. Chem. Soc.*, 2014, **136**, 17730–17733.
- 35 L. M. Pazos-Outón, M. Szumilo, R. Lamboll, J. M. Richter, M. Crespo-Quesada, M. Abdi-Jalebi, H. J. Beeson, M. Vrućinić, M. Alsari, H. J. Snaith, B. Ehrler, R. H. Friend and F. Deschler, *Science*, 2016, **351**, 1430–1433.
- 36 Y. Yamada, T. Yamada, L. Q. Phuong, N. Maruyama, H. Nishimura, A. Wakamiya, Y. Murata and Y. Kanemitsu, *J. Am. Chem. Soc.*, 2015, **137**, 10456–10459.
- 37 B. Wu, N. Huy Tiep, Z. Ku, G. Han, D. Giovanni, N. Mathews, H. J. Fan and T. C. Sum, *Adv. Energy Mater.*, 2016, **6**, 1600551.
- 38 X. Zhang, H. Liu, W. Wang, J. Zhang, B. Xu, K. L. Karen, Y. Zheng, S. Liu, S. Chen, K. Wang and X. W. Sun, *Adv. Mater.*, 2017, **29**, 1606405.
- 39 L. Zhang, X. Yang, Q. Jiang, P. Wang, Z. Yin, X. Zhang, H. Tan, Y. M. Yang, M. Wei, B. R. Sutherland, E. H. Sargent and J. You, *Nat. Commun.*, 2017, **8**, 15640.
- 40 X. Yuan, X. M. Hou, J. Li, C. Q. Qu, W. J. Zhang, J. L. Zhao and H. B. Li, *Phys. Chem. Chem. Phys.*, 2017, **19**, 8934–8940.

- 41 S. A. Veldhuis, P. P. Boix, N. Yantara, M. Li, T. C. Sum, N. Mathews and S. G. Mhaisalkar, *Adv. Mater.*, 2016, **28**, 6804–6834.
- 42 S. Kumar, J. Jagielski, S. Yakunin, P. Rice, Y.-C. Chiu, M. Wang, G. Nedelcu, Y. Kim, S. Lin, E. J. G. Santos, M. V. Kovalenko and C.-J. Shih, *ACS Nano*, 2016, **10**, 9720–9729.
- 43 J. Xing, F. Yan, Y. W. Zhao, S. Chen, H. K. Yu, Q. Zhang, R. G. Zeng, H. V. Demir, X. W. Sun, A. Huan and Q. H. Xiong, *ACS Nano*, 2016, **10**, 6623–6630.
- 44 B. M. D. Puscher, M. F. Aygueler, P. Docampo and R. D. Costa, *Adv. Energy Mater.*, 2017, **7**, 1602283.
- 45 W.-L. Hong, Y.-C. Huang, C.-Y. Chang, Z.-C. Zhang, H.-R. Tsai, N.-Y. Chang and Y.-C. Chao, *Adv. Mater.*, 2016, **28**, 8029–8036.
- 46 X. Zhang, H. Lin, H. Huang, C. Reckmeier, Y. Zhang, W. C. H. Choy and A. L. Rogach, *Nano Lett.*, 2016, **16**, 1415–1420.